2021 43rd Annual International Conference of the
IEEE Engineering in Medicine & Biology Society (EMBC)
Oct 31 - Nov 4, 2021. Virtual Conference

Design and Simulation of a Soft Robotic Device for Muscle Rehabilitation and Blood Flow Stimulation Therapy

Victor Ticllacuri[1,2] and Renato Mio[3]

***Abstract*— Previous works have shown the efficacy of mechanical stimulation by applying pressure and vibration on muscle rehabilitation. Additionally, a temperature increase can improve both muscle performance and blood circulation during therapies. These modalities of treatment are commonly applied separately in patients with moderate disuse-induced muscle atrophy. In this paper, we propose the design of a novel medical device that synergistically integrates the function of i) elastomeric pneumatic actuators to apply focused orthogonal pressure, ii) vibratory motors to generate localized vibration and iii) carbon fibre heaters for a temperature increase. In particular, computational simulations were performed to characterize the mechanical behaviour of different pneumatic actuator geometries and their predicted advantages in comparison to previous designs. The integration of the three functionalities of the device and preliminary simulations results showcase its potential for improving therapy efficacy, while also being compact, lightweight, and comfortable, which would ease its implementation in rehabilitation programs.**

***Clinical relevance*— Disuse-induced muscle atrophy and related cardiovascular problems can lead to physical impairment and significantly affect patient independence. The surge in the number of hospitalized and bedridden patients related to the coronavirus disease (COVID-19) brings about a predicted increase in the incidence of myopathies and muscle weakness. To attend the growing demand, technological aids for more efficient physical therapies will need to be developed.**

I. INTRODUCTION

Locomotion powered by lower-limb muscles enables people to perform several physical complex activities (e.g. walking, running and jumping). However, prolonged periods of inactivity or muscle disuse can negatively affect musculoskeletal and cardiovascular health [1]. A combination of muscle unloading and reduced neural activity occurs frequently in clinical settings following immobilization, which causes disturbances in protein turnover and leads to skeletal muscle hypotrophy [1]. Moreover, hospitalization, bed rest and physical inactivity related to the coronavirus disease 2019 (COVID-19 Pandemic) are greatly increasing the risk of musculoskeletal and neuromuscular damage. Current studies on COVID-19 patients report myopathies and neuromuscular damage as Intensive Care Unit (ICU)-acquired weaknesses (ICUAW) [2]. These conditions, together with other comorbidities (e.g. those related to diabetes, cancer, renal or heart failure and ageing) [3], can also lead to cardiovascular problems such as venous return-related pathologies (thrombosis and embolism), varicose veins, and ulcers [4], [5]; thus resulting in a more severe atrophy with critical consequences. This issue can lead to physical impairment and dependency; hence, it is necessary to treat disuse-induced atrophy efficiently by stimulating the skeletal muscles and promoting blood circulation in the lower limbs of patients.

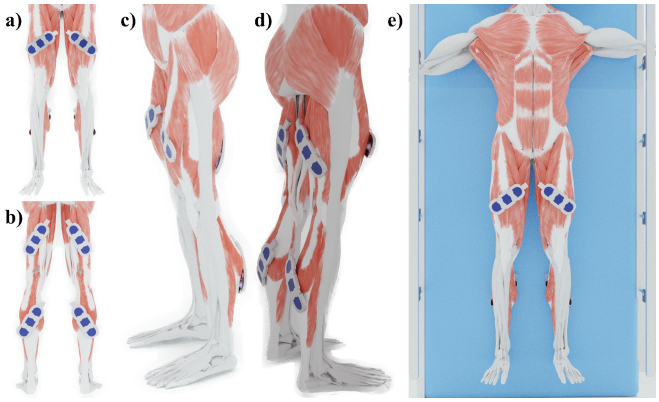

Fig. 1. Soft robotic device positioned in previously proposed strategic anatomical landmarks: Gastrocnemius, Semitendinosus, Semimembranosus, Biceps Femoris, Vastus Lateralis, Rectus Femoris, Sartorius, Vastus Medialis and Fossa Poplitea [6]. a) Front view. b) Back view. c) Frontal perspective view. d) Posterior perspective view. e) Top view of a patient lying in bed while using the device.

Current conventional treatments for disuse-induced atrophy involve resistance exercise and intensive physical activity [1]. However, many patients, especially elderly ones, are unable to exercise at a sufficient intensity to promote muscle growth. Additionally, these manual rehabilitation therapies are labor-intensive and time-consuming for both therapists and patients. On the other hand, invasive and non-invasive electrical muscle stimulation are also used as complementary technological treatment. These procedures often generate discomfort and insecurity in the patient due to the risks involved, such as misapplication and infections, in addition to not directly promoting blood circulation. Therefore, given the growing demand and predicted future needs, the development of new medical devices to treat disuse-induced atrophy becomes highly relevant.

Mechanical and thermal stimulation not only promote muscle development, but also stimulate blood flow and perfusion [7]–[10]. While most robotic devices for rehabilitation are mainly made of rigid materials, soft robotic devices (SRDs) offer the safety and comfort required for the

*This work was not supported by any organization

[1]Victor Ticllacuri is with the Biomedical Engineering Program PUCP-UPCH, Pontificia Universidad Catolica del Peru, Lima, Perú. victor.ticllacuri@pucp.edu.pe

[2]Victor Ticllacuri is also with the Biomedical Engineering Program PUCP-UPCH, Universidad Peruana Cayetano Heredia, Lima, Perú. victor.ticllacuri@upch.pe

[3]Renato Mio is with the Laboratory of Biomechanics and Applied Robotics, Pontificia Universidad Católica del Perú, Lima 15088, Peru r.mioz@pucp.edu.pe

interaction with the soft human tissues [11], [12]. However, to the authors' knowledge, there are no reported SRDs capable of performing external mechanical and thermal stimulation simultaneously or mimic manual therapy. With this aim, this paper presents the design of a SRD for lower-limb muscles and blood flow stimulation in patients with moderate disuse-induced muscle atrophy (see Fig. 1). The SRD comprises three modules: i) a set of elastomeric soft pneumatic actuators (SPAs) that apply orthogonal focused rhythmic pressure, ii) a circuit of carbon fibre heaters (CFHs) that promote an increase in the treated area's temperature, and iii) two coin-shaped vibration actuators (VAs) embedded on the SRD that generate localized vibration and further enhance the mechanical stimulation function. The modules are integrated in a case and multiple SRDs could be placed on different anatomical strategic landmarks (see Fig. 1).

II. Device Design

This section explains the design and integration of the SRD's three main interdependent modules.

A. Soft Pneumatic Actuators Design

The rhythmic application of an orthogonal force over a muscle generates a focused pressure that has biomechanical (i.e. reduction of muscle stiffness, increases of muscle strength, speed, and power), physiological (i.e. increases of blood flow and perfusion), and neurological (i.e. decreases of local pain and increases of muscle relaxation) therapeutic effects [7]. However, conventional robotic massagers are made of materials with low compliance, which limits the ergonomics and safety required for interaction with the soft human tissues [11], [12]. In this context, soft robotics are a feasible alternative for safe interaction with human muscle and skin [11]–[13], and to emulate the massaging motion patterns used in medical treatments [11], [12]. Therefore, the device's SPAs must be able to mimic therapeutic mechanical stimulation protocols and methods by applying focused orthogonal pressure over the skin and muscle.

Building upon previous works [6], [11], [13], three types of SPA with different geometries were designed parametrically (see Fig. 2a). Each SPA is made of two layers of the hyper-elastic Dragon Skin™ 30 silicone rubber (DSR) (Smooth On Inc.). This material was chosen for its higher Young modulus compared to other silicone materials [13], which allows the device to transfer more energy to the user and spend less in its own deformation. The layers are defined as those DSR membranes above the pneumatic chamber (top layer 'TL') and below it (bottom layer 'BL'), which have constant thicknesses T_{TL} and T_{BL} at the outer edges while their shapes near the pneumatic chamber do vary according to the type and model of SPA (see Fig. 2).

Furthermore, the pneumatic chamber was designed using the zero-air chamber (ZAC) concept (air chamber with "zero volume"), where the inner faces of the top and bottom layers are flush against each other, resulting in no useless air volume when the SPA is not being actuated [11] (see Fig 2a). This arrangement is highly compact and lightweight, in addition

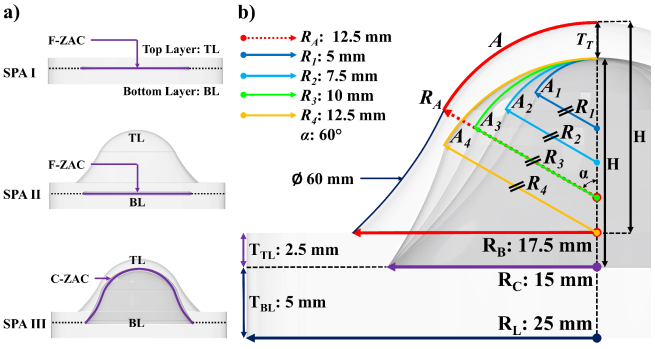

Fig. 2. SPA variations. a) Lateral view of the SPAs showcasing different top and bottom layer geometries, as well as pneumatic chamber shapes b) Lateral view of the SPAs II and III main dimensions. On SPA-III variations, only R_n and the arc A_n center are varied while the other dimensions are kept constant.

to simplifying the manufacturing process, preventing delays and avoiding waste of energy in the chamber initial pressurization. Then, as pressurised air enters into the pneumatic chamber, its volume increases, deforming its top and bottom layers. The top layer deformation exerts the orthogonal focused pressure for the required mechanical stimulation on the patient's skin and muscle. The three different SPA geometries are described in the following paragraphs.

1) SPA type I (SPA-I): It consists of two flat circular DSR layers TL and BL with radius R_L (see Fig. 2a). It has a Flat Zero-Air Chamber (F-ZAC) with radius R_C between the DSR layers. This simple design makes the SPA compact with a total thickness of only 7.5 mm (T_{TL}+T_{BL}). This type of SPA is based on previous works [6], [11], [13] and it will serve as a baseline model for the comparative analysis with the other SPA types.

2) SPA type II (SPA-II): Similar to SPA-I, as it keeps the two DSR layers with radius R_L as well as the F-ZAC with radius R_C between both layers. However, TL now incorporates a DSR bell-shaped profile described by arc A (see Fig. 2b). This arc is determined by its radius R_A and the arc angle alpha, and it is centered 2.5 mm above the top layer's level. In addition, the lower end of the arc A is connected to the top layer's level by a 60 mm diameter arc (see Fig. 2b). The purpose of this bell-shaped profile is to passively generate local pressure on the skin and muscles when the SPA is fitted on the patient's limbs. When actuated, the focused pressure will increase further.

3) SPA type III (SPA-III): As in SPA-II, the two DSR layers with radius R_L are kept, as well as the bell-shaped outer profile. However, the F-ZAC is now replaced by a Curved Zero-Air Chamber (C-ZAC) described by the arcs A_n, where n is a positive integer ranging from 1 to 4 (Fig. 2b), referring to the four geometric configurations of SPA-III designed for this study in which only the arc radii and their centres were varied while the other dimensions are kept constant. The arc A_n higher end starts at 12.5 mm above the top layer's level and is 2.5 mm below the top of arc A. This means that thickness T_{TL} is preserved at the top to carry out a comparative analysis with the other types of SPA. The arcs A_n are determined by their radii R_n and arc angle α, and

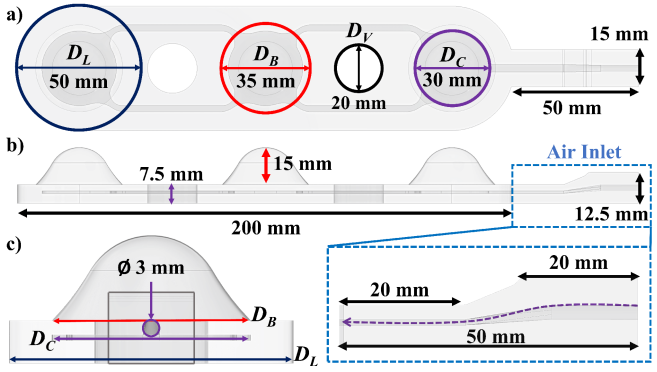

Fig. 3. Configuration of 3 SPAs integrated in the DSR matrix. a) Top view of the SPAs integrated in the SPA Matrix. b) Side view of the integration. c) Posterior view of the nozzle for the air inlet and the SPAs. D_L: Diameter of layers D_B: Diameter of the bell D_C: Diameter of the pneumatic chamber D_V: Diameter for the VAs.

they are centered at a height $(4-n)T_{TL}$ mm with respect to the top layer's level. A constant 60 mm diameter arc connects the lower ends of A_n with the top layer's lower face.

Each SRD comprises an array of 3 SPAs of the same type integrated in a DSR matrix (see Fig. 3). This soft component includes 20 mm diameter holes between each SPA where the VAs should be inserted (see Fig. 3a). For the SRDs to actuate over the proposed muscle's sizes, the design of the matrix is based on the anthropometric measurements of the 95% upper percentile of Peruvian men according to the National Health Institute of Peru (see Fig. 1). In addition, the matrix includes a nozzle for the pressurised air inlet to the pneumatic chambers (see Fig. 3b). Its dimensions were determined ensuring adequate clamping and airtightness (see Fig. 3c). In order to allow a higher velocity and uniform flow, the air channels between the pneumatic chambers follow smooth trajectories (see Fig. 3a).

B. Carbon Fibre Heater

An increase in lower limb muscles' temperature can be attained by heating the device in contact with the skin within safe limits. This temperature increase would improve not only muscle performance in speed, strength, power and muscle recruitment (see Table 1), but would also improve blood flow and perfusion in these areas [5], [10], mainly due to the temperature-induced vasodilation. The CFH shown in Fig. 4 is made of Hots™ Double Layer Carbon Fiber Heating Wire which must be able to increase its temperature by 15°-30°C around the area with which the SRD is in contact for it to produce the benefits listed in Table 1. The operation of the CFH is based on the joule effect. In this way, a relationship between electrical power and temperature sensed in the device can be defined. For safety reasons, a maximum voltage of 220 VAC is considered to generate the power at the CFH for the temperature variation.

The CFH design is based on a configuration analogous to radiators (see Fig. 4) to maximize the heat generation per unit area. Furthermore, this cable is embedded in a thermally conductive and electrically insulating polymeric matrix (Epoxies™ 50-1225 Thermally Conductive Silicone Rubber) in order to direct the heat towards the user and not towards other components matrix comprises a heating unit of the CFH (see Fig. 4). The device comprises six heating units that are located at the periphery of the device in order to cover and increase the temperature over a larger area, as well as to prevent overheating of the device electronics mounted on its center.

C. Vibration actuators

The application of localized vibration in the lower limb has the potential to improve muscle performance [8], [9], depending on the vibration frequency (Hz) and the vibratory load (m/s), in terms of force, speed, power and blood perfusion (see Table 1). Then, the VAs must be able to generate localised surface vibration in a frequency range between 10 to 300 Hz for the device to foster the benefits listed in Table 1. Therefore, the VAs chosen are two "Pico-Vibe ©" model 312-103 coin-shaped vibratory motors (see Fig. 4), which are compact, voltage-controlled and can attain the required vibration frequency ranges.

The VAs are inserted between the thermally non-conductive silicon matrix of the SPAs to isolate them from the heat dissipated by the CFHs. Due to the location of the VAs with respect to the SPAs, both types of actuators work in coordination by applying localised vibration and focused pressure simultaneously, effectively performing mechanical muscle stimulation.

D. Device integration

A case was designed considering proper placing of all components, wiring channels for power supply and easy assembly (see Fig. 5). The case aims to ensure interdependent operation between actuators, device and patient safety by thermally and mechanically isolating electronic components, and minimizing of the overall size of the device (see Fig. 6a). SPAs are fixed on supports that hold the matrix in place and aid in directing the pneumatic chamber deformation and

TABLE I. Physiological responses induced by mechanical and thermal stimulation

Aspect improved by	Δ Temperature	Vibration frequency/load
Muscle force/strength	15-25 °C [10]	10-300 Hz [9]
Muscle power	20-30 °C [10]	50-150 Hz [9]
Muscle speed	15-20 °C [10]	30-80 Hz [9]
Muscle recruitment	15-25 °C [10]	-
Blood perfusion	-	150 m/s [8], [9]

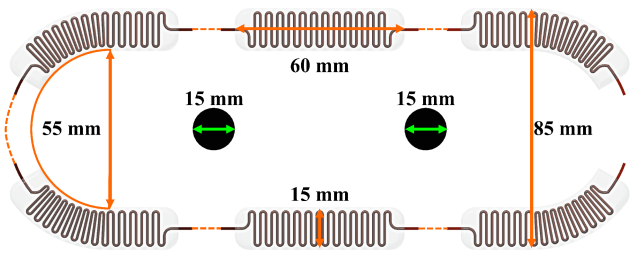

Fig. 4. Dimensions and configuration of the six units of the CFH and the two VA motors. VA thickness: 3 mm. Note that the carbon fibre cable is embedded in the silicone matrix.

applied pressure towards the user's limb efficiently (see Fig. 5). Finally, the device is secured by screws on the side and front. The SRD weights approximately 350g, a low value given the use of soft, low-density materials.

III. Methods

Finite element analysis (FEA) simulations were performed using ANSYS Workbench 2020 R2 software. All SPA geometries with and without a rigid support were subjected to a static inflation simulation (see Fig. 7). Conditions were set to simulate a 100 kPa inlet maximum pressure for each pneumatic chamber wall with a fixed support in the SPA's external lateral sides. This last condition represents the SPA being enclosed by the rigid case.

The SPA material was DSR (Tensile Yield Strength: 3.44 MPa), Mooney-Rivlin 3-parameter hyperelastic model and the support material was Polyethylene Terephthalate, also know as PET plastic (Tensile Yield Strength: 52.44 MPa). Von Misses equivalent stress, static safety factor, total and directional deformation of the SPA's whole body as well as the top layer's membrane (M_{TL}) and the bottom layer's membrane (M_{BL}) were the analyses performed.

For a comparative energy efficiency analysis, an energy ratio (ER) is defined as the ratio between the total deformation (TD) towards the user and the total deformation in any direction, expressed in equation 1:

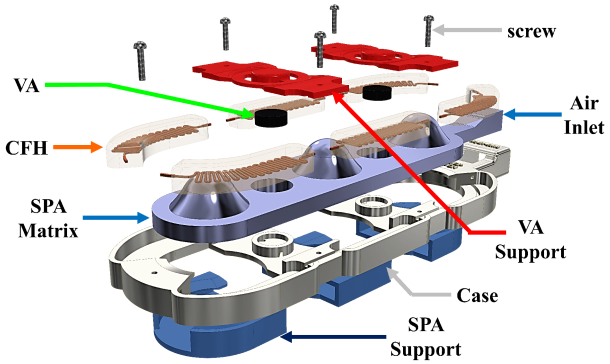

Fig. 5. Exploded view of the SRD.

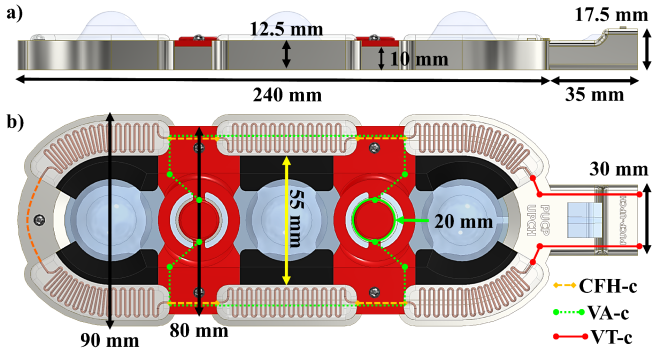

Fig. 6. a) Lateral and b) top view of the SRD. Colored lines display channels for the cables of CFH (CFH-c), VAs (VA-c) and shared channels for VAs and CFH wiring (VT-c)

$$ER = \frac{TD_{TL}}{TD_{TL} + TD_{BL}} \quad (1)$$

Where TD_{TL} and TD_{BL} are the total deformations of M_{TL} and M_{BL} respectively. An energy ratio close to 100% means that most of the pneumatic energy is directed towards the patient's muscles.

IV. Results and Discussion

Fig. 7a shows the set-up for the simulation of the SPA with PET supports. In all the simulations, the SPA supports had a minimum safety factor of at least 13.5. Figures 7c and 7d show the directional deformations (DD) of M_{TL} and M_{BL} for SPAs without and with a lower support respectively each type of SPA. Note that for both Fig. 7c and Fig. 7d, the top layer's amplitude A_{TL} (the total distance from the top layer's level to the top of the bell profile when actuated) has the same values for their respective SPA types, meaning that the SPA supports does not affect SPA performance.

Table 2 shows the directional deformation of M_{TL} and the value of A_{TL} for every SPA. SPA-I has the largest directional deformation when actuated given that its M_{TL} has a lower thickness when compared to the SPAs with a bell-shaped profile. Regarding the SPA-III variations, model 4 has a greater directional deformation than the other models. The SPA-II model has the largest A_{TL}, and both types II and III have greater A_{TL} than the conventional SPA-I, mainly due to the bell-shaped profile incorporated which passively increases their amplitudes. These deformations comparisons show that passive actuation by the bell-shaped profile and active SPA deformation would produce mechanical stimulation at greater depth than conventional flat SPAs. Moreover, the adding of a rigid support greatly improves function as seen in Fig. 7c, which shows clear deformations on M_{TL} for the SPA without a rigid support, while in Fig. 7d it can be seen how the SPA with support shows negligible deformation in its M_{BL}.

Fig. 7b shows the stress distribution in the three types of SPA. In all cases, the maximum equivalent stress is found in the circumferential edges of the pneumatic chamber side walls, as this is where the SPA is most susceptible to failure [11], [13] due to the tearing of the silicone layers by the hyper-elastic deformation of the DSR layers. SPA-II has the lowest maximum stress (and highest safety factor) given that the bell-shaped profile over the F-ZAC limits the excessive deformation of the upper membrane. SPA III-3 has the second best safety factor, as its membrane has the same thickness throughout the bell profile (Table 2). Finally,

TABLE II. FEA simulations results for each SPA

SPA Type	TL DD (mm)	A_{TL} (mm)	ER (%)	SF
SPA I	7.32	7.32	99.04	1.96
SPA II	1.57	16.57	94.42	3.99
SPA III-1	0.86	15.86	95.67	3.08
SPA III-2	0.90	15.90	96.17	3.56
SPA III-3	1.08	16.08	96.68	3.69
SPA III-4	1.18	16.18	97.18	3.03

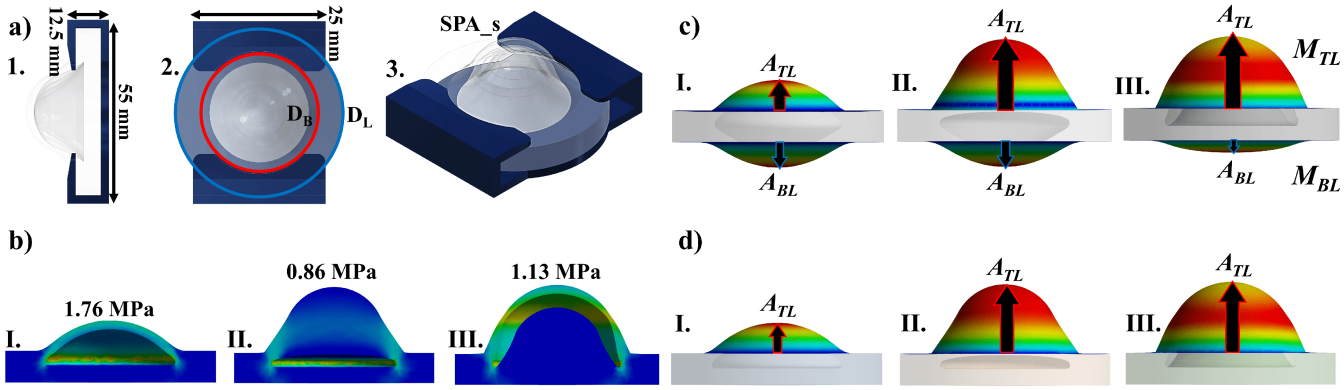

Fig. 7. FEA simulations of the SPA types. a) SPA and the SPA support configuration side, top and perspective views. b) Cross-section view of stress distribution for the 3 types of SPA when subjected to pneumatic pressure. The text on top specifies the maximum stress. c) Directional deformation (on the vertical axis) for the SPA variations without and d) with rigid support.

SPA-I has highest ER, mainly due to their layers' constant thicknesses instead of a bell-shaped profile; resulting in greater deformations at the same applied pressure. Amongst the other SPA geometries, SPA III-4 has the next highest ER, probably due to having a thinner top layer.

V. Conclusions and Future Work

The design of a soft robotic device that incorporates different modalities of treatment aimed for muscle rehabilitation and blood flow stimulation was proposed. The device synergistically integrates three pneumatic actuators, two vibratory actuators and a carbon fibre heater to produce mechanical and thermal effects which have proved efficacy in improving muscle performance and blood flow stimulation. The device meets technical and usability requirements by being compact, modular, lightweight, and safe.

FEA simulations showed that SPA-II has greater potential for applying pressure (higher A_{TL}) and the best safety factor. However, all the SPA-III models have a higher ER at similar A_{TL} values. Therefore, it can be said that both types of SPA have similar performances and either could be preferred depending on whether mechanical resistance or energy efficiency are prioritized. Furthermore, the use of a bell-shaped profile in SPA-II and SPA-III could aid in passively applying pressure on the tissue upon fitting the device and a greater mechanical stimulation through pneumatic actuation.

The use of this device in physical rehabilitation therapies could be of great aid for patients suffering ICUAW in achieving a faster recovery and attend the predicted increase in number of cases due to immobilization conditions related to the COVID-19 pandemic. However, a possible limitation is the magnitude of the maximum pressure and temperature that the device could generate to produce the physiological stimulus and responses.

Finally, as next steps, the mechanical behavior of the SPAs' interaction with skin and muscles will be assessed through simulations for further optimization of the design. The device fabrication and validation will be performed and, particularly, the SPAs will be characterized experimentally to determine an accurate control relationship between the input air pressure and the orthogonal force output.

Acknowledgments

The authors would like to thank Midori Sanchez for her advice in the choosing of the device materials, and Katherine Hinostroza for her help in rendering some of the figures.

References

[1] Y. Gao, Y. Arfat, H. Wang, and N. Goswami, "Muscle atrophy induced by mechanical unloading: Mechanisms and potential countermeasures," *Frontiers in Physiology*, vol. 9, 3 2018.

[2] S. Bagnato, C. Boccagni, G. Marino, C. Prestandrea, T. D'Agostino, and F. Rubino, "Critical illness myopathy after covid-19," *International Journal of Infectious Diseases*, vol. 99, pp. 276–278, 10 2020.

[3] S. K. Powers, G. S. Lynch, K. T. Murphy, M. B. Reid, and I. Zijdewind, "Disease-Induced Skeletal Muscle Atrophy and Fatigue," *Medicine Science in Sports Exercise*, vol. 48, nov 2016.

[4] M. D. Nisio, N. van Es, and H. R. Büller, "Deep vein thrombosis and pulmonary embolism," *The Lancet*, vol. 388, 12 2016.

[5] Y. K. Jan, S. Shen, R. D. Foreman, and W. J. Ennis, "Skin blood flow response to locally applied mechanical and thermal stresses in the diabetic foot," *Microvascular Research*, vol. 89, pp. 40–46, 9 2013.

[6] V. Ticllacuri, G. J. Lino, A. B. Diaz, and J. Cornejo, "Design of wearable soft robotic system for muscle stimulation applied in lower limbs during lunar colonization," in *2020 IEEE XXVII International Conference on Electronics, Electrical Engineering and Computing (INTERCON)*, pp. 1–4, 2020.

[7] P. Weerapong, P. A. Hume, and G. S. Kolt, "The mechanisms of massage and effects on performance, muscle recovery and injury prevention," *Sports Medicine*, vol. 35, pp. 235–256, 9 2005.

[8] J. T. Fuller, R. L. Thomson, P. R. C. Howe, and J. D. Buckley, "Effect of vibration on muscle perfusion: a systematic review," *Clinical Physiology and Functional Imaging*, vol. 33, 1 2013.

[9] A. Alghadir, S. Anwer, H. Zafar, and Z. Iqbal, "Effect of localised vibration on muscle strength in healthy adults: a systematic review," *Physiotherapy*, vol. 104, 3 2018.

[10] L. C. Rome, "Influence of temperature on muscle recruitment and muscle function in vivo," *American Journal of Physiology-Regulatory, Integrative and Comparative Physiology*, vol. 259, 8 1990.

[11] P. Vela-Anton, C. Nina, V. Ticllacuri, D. Shah, J. Tincopa, M. Llontop, F. Aguilar, S. Cruz, and E. Vela, "Borjibot: A soft robotic device performing pressure and torsional stimuli for neonates oral-motor rehabilitation," in *2020 8th IEEE RAS/EMBS International Conference for Biomedical Robotics and Biomechatronics (BioRob)*, pp. 403–409, 2020.

[12] M. Cianchetti, C. Laschi, A. Menciassi, and P. Dario, "Biomedical applications of soft robotics," *Nature Reviews Materials*, vol. 3, 6 2018.

[13] J. J. Huaroto, V. Ticllacuri, E. Suarez, R. Ccorahua, and E. A. Vela, "A soft pneumatic haptic actuator mechanically programmed for providing mechanotactile feedback," *MRS Advances*, vol. 4, no. 19, p. 1131–1136, 2019.